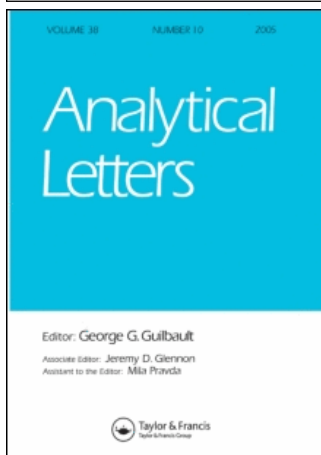


This article was downloaded by:[Conger, Robert]
On: 18 September 2007
Access Details: [subscription number 782129110]
Publisher: Taylor & Francis
Informa Ltd Registered in England and Wales Registered Number: 1072954
Registered office: Mortimer House, 37-41 Mortimer Street, London W1T 3JH, UK



Analytical Letters

Publication details, including instructions for authors and subscription information:

<http://www.informaworld.com/smpp/title~content=t713597227>

Analysis of the Acid Passivation of Stainless Steel

C. O'Laoire ^a; B. Timmins ^b; L. Kremer ^c; J. D. Holmes ^a; M. A. Morris ^a

^a Department of Chemistry, University College Cork, Cork, Ireland

^b OMC Scientific Ltd, Limerick, Ireland

^c Stellar Solutions, Algonquin, Illinois, United States

Online Publication Date: 01 August 2006

To cite this Article: O'Laoire, C., Timmins, B., Kremer, L., Holmes, J. D. and Morris, M. A. (2006) 'Analysis of the Acid Passivation of Stainless Steel', *Analytical Letters*, 39:11, 2255 - 2271

To link to this article: DOI: 10.1080/00032710600755363

URL: <http://dx.doi.org/10.1080/00032710600755363>

PLEASE SCROLL DOWN FOR ARTICLE

Full terms and conditions of use: <http://www.informaworld.com/terms-and-conditions-of-access.pdf>

This article maybe used for research, teaching and private study purposes. Any substantial or systematic reproduction, re-distribution, re-selling, loan or sub-licensing, systematic supply or distribution in any form to anyone is expressly forbidden.

The publisher does not give any warranty express or implied or make any representation that the contents will be complete or accurate or up to date. The accuracy of any instructions, formulae and drug doses should be independently verified with primary sources. The publisher shall not be liable for any loss, actions, claims, proceedings, demand or costs or damages whatsoever or howsoever caused arising directly or indirectly in connection with or arising out of the use of this material.

Analytical Letters, 39: 2255–2271, 2006
Copyright © Taylor & Francis Group, LLC
ISSN 0003-2719 print/1532-236X online
DOI: 10.1080/00032710600755363



SURFACE ANALYSIS

Analysis of the Acid Passivation of Stainless Steel

C. O'Laoire

Department of Chemistry, University College Cork, Cork, Ireland

B. Timmins

OMC Scientific Ltd, Limerick, Ireland

L. Kremer

Stellar Solutions, Algonquin, Illinois, United States

J. D. Holmes and M. A. Morris

Department of Chemistry, University College Cork, Cork, Ireland

Abstract: Passivation of 304 and 316 stainless steels in various acid solutions was studied as a function of exposure time and acid concentration. Nitric acid, citric acid, and the commercial Citrisurf (a commercial citric acid-based passivating solution, Stellar Solutions, USA) were compared. The materials were studied by low-angle PXRD (powder x-ray diffraction), XRF (x-ray fluorescence), SEM (secondary electron microscopy), and XPS (x-ray photoelectron spectroscopy). As might be expected, the measurements showed increased Cr:Fe ratios at the surface following acid passivation. Using the combination of characterization methods, it was possible to generate concentration-depth profiles, and these suggest that chromium enrichment can penetrate several micrometers into the surface for nitric acid treatment, and this is related to some surface damage. The low-angle PXRD work illustrated that complex phases are formed at the passivated surface, and these phases exhibit a rich structural chemistry. It is concluded that citric

Received 28 February 2006; accepted 20 March 2006

Address correspondence to M. A. Morris, Department of Chemistry, University College Cork, Cork, Ireland. Tel.: 353 21 4902180; Fax: 353 21 427094; E-mail: m.morris@ucc.ie

acid-based passivating agents result in more coherent oxide surfaces that are more resistant to corrosion.

Keywords: Surface analysis, X-ray analysis, passivation, corrosion, surface oxidation

1. INTRODUCTION

Acid passivation of stainless steels is widely used in industry to improve the corrosion resistance of the materials through the creation of coherent surface oxide films. This technique has particular importance in the chemical, pharmaceutical, food, and medical implant sectors. The passivation process has been discussed many times and authors such as Maller (1998) have summarized most of the important aspects. The surfaces of the materials show enhanced chromium content due to preferential dissolution of iron oxide (Olsson and Landolt 2003). Surface Cr_2O_3 films are advantageous because of their inherent corrosion resistance, low ion/electron diffusivities, and low electrical conductivity (Maller 1998; Askeland 1985). Passivation of stainless steels by nitric acid is common, but citric acid-based passivation is now an acknowledged competitive process. Citric acid passivation is a well-established technique in the beverage industry since it is more effective (than the mineral acids) in reducing trace iron in contacting solutions (Hicks 1995). In citric acid-based passivating solutions, it is thought that the additional chelating power of the citrate anion selectively enhances iron removal (Roll 1996). Modern proprietary citric acid-based passivating solutions (such as Citrisurf used here) also contain chelating agents and surfactants to enhance the complexing and wetting properties of the solutions. The advantage of these solutions is that because of their (in comparison to nitric acid) biodegradability and low Ni, Cr, Mn, etc., content, they can be charged to a standard sewer system.

However, despite the widespread use of citric acid passivating agents and their proven efficacy, there are relatively few detailed quantitative studies of the changes in the surface composition and structure as a function of treatment. This paper uses a combination of several material analysis methods to study changes in the surface of stainless steels on exposure to three different passivating agents. In particular, we demonstrate that nondestructive depth profiles can be generated using this combination of analytical methods and believe this approach could be used in many areas of materials analysis.

2. EXPERIMENTAL

Powder X-ray Diffraction (PXRD) measurements were made using a PANalytical X Pert PRO diffractometer equipped with a Cu anode (40 kV and

30 mA power conditions) and nickel mask. Programmable divergent slits coupled with anti-scatter slits were used together with incident and reflection Göbel mirrors. An X'Celerator detector was used in scanning mode using an active length of $2.122^\circ 2\theta$. Data were collected in standard $\theta - 2\theta$ reflection mode (i.e., incident and scattered angles are θ) and at fixed angles of incidence (ω) to enhance surface sensitivity (1, 5, and $10^\circ \omega$ to the surface plane). X-ray fluorescence (XRF) data were collected on a standard Philips MiniPal flushed continuously with helium. In all cases, a Rh anode was used. Samples were generally mounted in a Teflon holder to reduce the low energy background. A 45° angle was maintained between the sample and the detector. For collection of K lines, the Rh anode was used at 20 kV and $15 \mu\text{A}$. For L-edge data, the samples were mounted in an aluminium holder. Low energy data were collected at anode settings of 5 kV and $100 \mu\text{A}$ and curve-fitting was required to separate Cr and Fe contributions. XRF and XRD data were quantified using software developed in-house. Very simply, it is a layer-by-layer model that calculates the emerging intensity from the sample as a function of depth. The fluorescence yields from the atoms n^{th} atomic layer are calculated according to estimated concentrations. The fluorescent yields through the layers above it ($n = 0$ is the outermost atomic layer) are then estimated. Similar calculations are made for the $n^{\text{th}}-1$, $n^{\text{th}}-2$, $n^{\text{th}}-3$, ... $n = 0$ layer until the total intensities can be estimated by integration. The value of n is varied until the point where the signal estimated at n atomic layers is within 0.1% of that at $2n$. Fluorescence yields are estimated from values given in Krause (1979) and mass absorption coefficients from the National Bureau of Standards (McMaster et al. 1969). The software also allows the addition of layers of differing composition to the outer surface so as to allow effects such as segregation to be modelled. Secondary Electron Microscopy (SEM) data were collected using JSM-5510 apparatus (JOEL) at a beam voltage of 25 kV. X-ray Photoelectron Spectroscopy (XPS) data were collected on a Vacuum Generators instrument using an $\text{AlK}\alpha$ source and a pass energy of 50 eV.

X-ray Photoelectron Spectroscopy next, 2 cm^2 (about $1.5 \times 1.5\text{-cm}$ pieces) metal coupons (2 mm thick) were machined from 316 and 304 stainless steel. The coupons were mechanically polished and precision lapped to a mirror finish. The surfaces were then polished using progressive 25, 10, and $5 \mu\text{m}$ diamond pastes and cleaned ultrasonically at $50\text{--}55^\circ\text{C}$ in acetone, water, and, finally, absolute alcohol to remove all traces of contamination. Solutions of nitric acid (NA), citric acid (CA), and Citrisurf 2250 (CS) passivating agents were prepared by dilution at various weight concentrations (% w/w). Coupons were exposed to varying solutions for different exposure times and concentrations. In all cases, the temperature was maintained at 50°C during passivation. Citrisurf is a commercial chelating passivating agent available from Stellar Solutions, Illinois.

3. RESULTS

3.1 XRF Measurements

No silicon or other low-concentration additives such as P and Na could be observed; consequently, the measurements refer to metal content only. The measured Cr:Fe K line peak area ratios in the 304 and 316 coupons are 0.38 and 0.42, respectively. The Cr:Fe L3 peak area ratios were measured at about 0.21 and 0.19 for 316 and 304 steel coupons, respectively. The high K line peak area ratio observed is not due to extensive segregation but rather to a lower absorption coefficient for Cr $K\alpha$ x-rays in iron compared to Fe $K\alpha$ x-rays in the same material. Using the quantifiable model described above, the values of the Cr:Fe atomic ratio can be estimated as 19.5 and 17 atomic % for 304 and 316, respectively (the measured Cr:Fe $K\alpha$ peak area ratio is larger for 316 because of the higher content of Mn and Ni in this alloy). These values are consistent with the values observed by L line analysis, which can be used to estimate bulk concentrations of 19.2 and 16.5 atomic % (316 and 304, respectively). The estimated values are fully consistent with ASTM standards for these steels. It is clear that XRF largely reflects the bulk concentrations of the metals. From the known absorption coefficients (Krause 1979; McMaster et al. 1969), an estimate of the "escape depth", or more correctly the mean free path, can be made (the depth when the signal emerging at the surface is $1/e$ of the total). For Cr K x-rays in iron, this depth is around $3.95\ \mu\text{m}$. The L lines originate from much deeper in the sample since they cannot excite the K-edge transitions.

Exposure to passivating solutions resulted in significant increases in the Cr:Fe K line peak area ratio within the x-ray – defined analyte for both 304 and 316 stainless coupons (there was no change in the L line ratios since these represent a true bulk ratio and no enrichment was observable at this depth). The results are summarized in Fig. 1 as Cr:Fe atomic ratio against acid concentration for an exposure to acid time of 3 h. The accuracy of the measured atomic ratio is around ± 0.025 . It can be seen that concentration is important; however, within the limits of experimental error, the optimum concentration of acid is around 10–20%, with higher concentrations having relatively small effects and, in some cases, deleterious effects (e.g., 316 stainless steel in nitric acid). It can also be seen that the Citrisurf allows either the 304 or 316 samples to reach the optimum Cr:Fe ratio at 5% dilutions. For both steels, the nitric acid shows a tendency to produce the highest Cr:Fe ratio at the highest concentrations. It is argued below that this is due to the formation of a deeper surface chromium-enriched area.

Within this exposure regime, it can be seen that all acids produce chromium-enriched materials. The amount of enrichment is relatively small, and quantification suggests a value of 3 to 6% dependent on

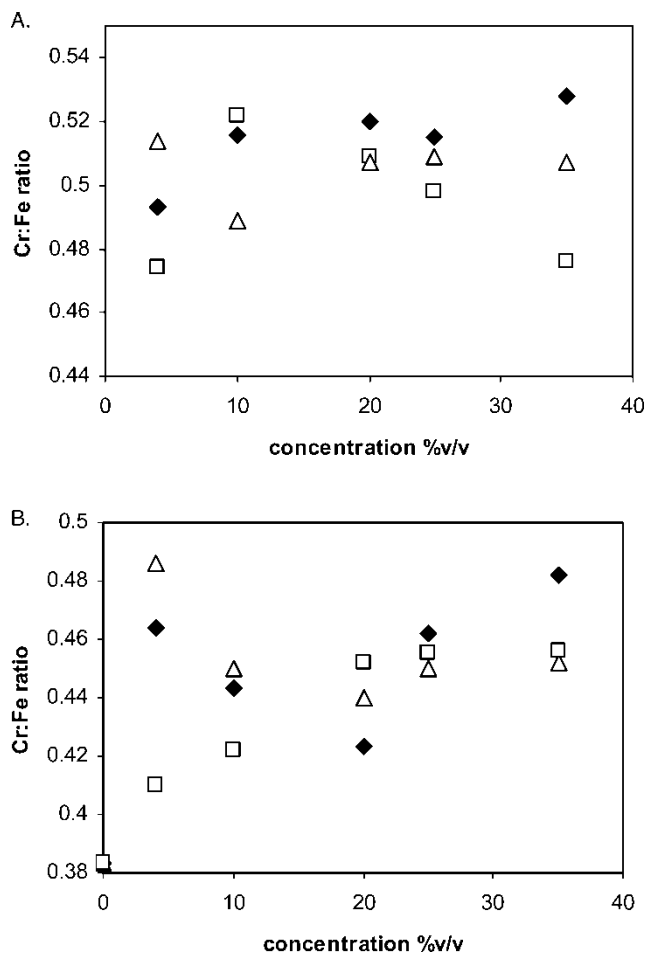


Figure 1. XRF determined Cr:Fe atomic ratios after 3 h exposure to passivating solutions of various concentrations. (A) Data from passivation of 316 stainless, ◆ = nitric acid; □ = citric acid, and △ = Citrisurf. (B) same as (A) except 304 stainless coupon.

conditions. It is apparent that 316 stainless steel reaches a measurably greater Cr:Fe ratio (as measured by XRF) than the 304 version. It should also be pointed out that the citric acid and Citrisurf passivating agents tended to reach a limiting value of chromium enrichment and that passivating time and concentration (above 10% solution values) had little effect. This was not true for nitric acid, where we found that extended exposures also increased the Cr:Fe ratio determined by XRF. For example, it was found that a 24-h exposure to 30% nitric acid resulted in a measured enrichment of about 11%.

3.2 PXRD Measurements

PXRD analysis provided very detailed analysis of the passivation process, and, in particular, the fixed low angle of incidence data provided significant advances in the study of these materials. In general, all the PXRD profiles were dominated by the austenitic steel structure (γ -phase), with the (111) and (200) features at 43.69 and 50.63 $^{\circ}2\theta$ being the most apparent (data referenced to JCPDS file 31-0619). The 2θ range of about 30 to 55 $^{\circ}$ provides the range most suitable for analysis of these materials. Typical data for an untreated surface (304) are shown in Fig. 2(A). Traces of an iron-rich martensitic phase (α -phase) can also be detected [(110) reflection at 44.64 $^{\circ}2\theta$, as referenced according to JCPDS file 44-1292]. On 316 stainless steel, exposure to all of the passivating solutions, the intensity of the α -phase decreased to a level that was barely detectable. This was not apparent for treatments of 304 coupons in which the martensitic phase was much more apparent. Also visible on the untreated surfaces was a Fe_3O_4 (37.4 $^{\circ}2\theta$, JCPDS file 75-0449) phase, but this was variable depending on surface pretreatment.

3.2.1 316 Coupon Analysis

Typical PXRD data for 316 materials exposed to the acid solutions (20%) for 6 h at a 10 $^{\circ}$ ω angle are shown in Fig. 2B and major phases are indicated. Obvious at these incidence angles is a peak at 39.85 $^{\circ}2\theta$, indicative of the corundum phase of chromium oxide, Cr_2O_3 (JCPDS file 74-0326). Enhanced surface sensitivity at lower incidence angles can be achieved. Typical data are shown in Fig. 2(C) for 5 $^{\circ}$ ω angles for exposure to 20% Citrisurf solution as a function of time. It is possible to observe in these data additional phases such as a Cr_{26}C_6 carbide phase (36.8 $^{\circ}2\theta$, JCPDS file 03-1176) and a spinel phase (35.7 $^{\circ}2\theta$ FeCr_2O_4 , JCPDS file 24-0512). Seen in other data are features at 41.4 $^{\circ}2\theta$ and 47.0 $^{\circ}2\theta$ assigned to an Fe_2O_3 phase (JCPDS file 75-0449). A CrO_2 phase can also be observed at 36.85 $^{\circ}2\theta$ (JCPDS file 43-1040). The observation of a chromium carbide phase is surprising. It is most easily observed in Citrisurf treatments and may be due to reaction of some of the additives with exposed and, thus, chemically active chromium during preferential dissolution of iron. The formation of spinel phases was first suggested by McBee and Kruger (1972), and this has been confirmed in more recent work (Lister et al. 1987). The Fe_2O_3 might be expected as a corrosion product and FeMo phases could be expected for 316 steels, and it is only observed in the study of this steel.

Data from Fig. 2C can be used to follow the development of the passive film with time for each of the passivating agents (Fig. 3). The plots are drawn as a normalized peak area intensity [to the austenitic (111) reflection] against exposure time. For all of the passivating agents used, there was an increase in the total PXRD signal as a function of exposure, presumably due to dissolution of organic amorphous material such as contamination and processing

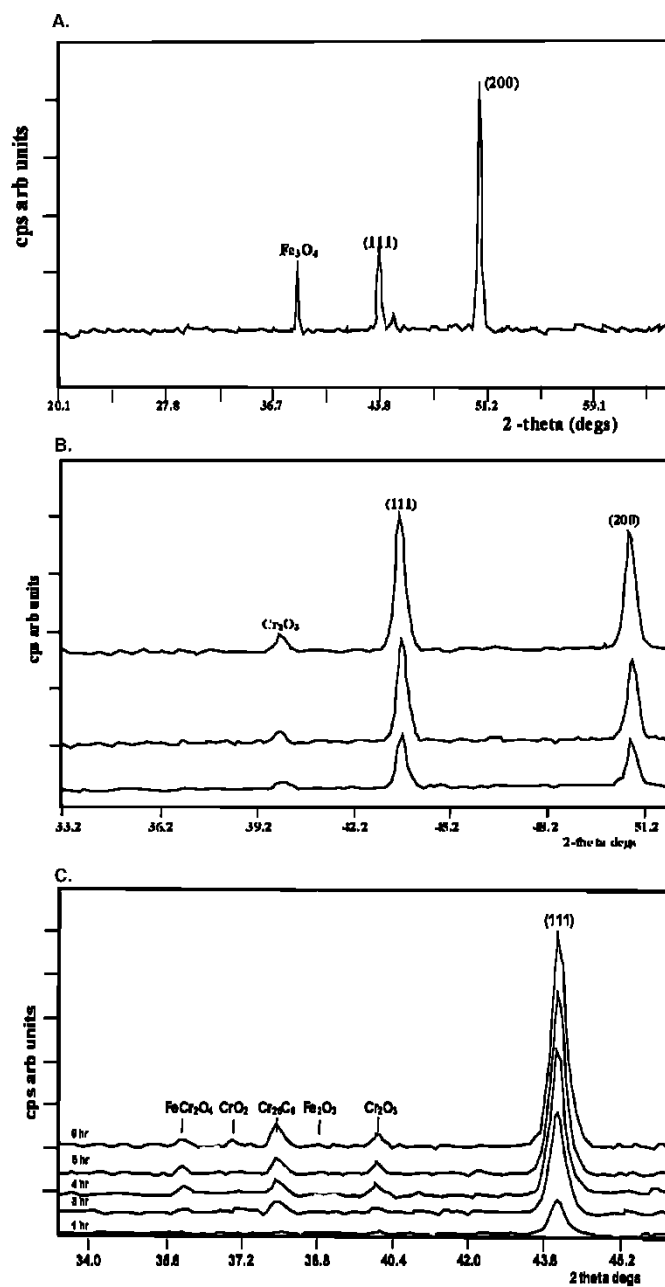


Figure 2. Typical PXRD data for materials described here. (A) Data from an unpassivated 304 surface. (B) The effects of passivation of 316 in each solution as indicated (20%, 6h). (C) Data from a Citrisurf passivated 316 coupon as a function of time (as described in figure).

products. The development of the spinel FeCr_2O_4 , Cr_{26}C_6 , CrO_2 , Cr_2O_3 , and Fe_2O_3 phases can be easily observed. For Citrisurf (Fig. 3A), there is a rapid decrease of a Fe_2O_3 signal to about 1/20 of the untreated value after 2 h. Peaks of chromium oxide (Cr_2O_3 and CrO_2) and spinel phases grow on acid exposure, and all of these phases display a maximum intensity after 1 h, which then decreases to an almost constant value after 2 h exposure. The maximum intensity observed is consistent with accepted views of the nature of passive films formed on stainless steels. It is generally accepted that the outermost layer is an iron oxide/hydroxide – rich layer (Calinski and Strehblow 1989; Kirchheim et al. 1990). In the center of the passive film, strong enrichment of chromium is seen; before the base of the film closes to bulk metal, the oxide has a cation stoichiometry close to that of the metal (Calinski and Strehblow 1989; Kirchheim et al. 1990). Surface stoichiometry measurements suggest the chromium-rich component may consist largely of chromium spinel phases (Lister et al. 1987). It appears that the Citrisurf passivation (0–1 h) initially dissolves the iron-rich outermost surface, leading to increased intensity in all the subsurface chromium phases. The PXRD data presented here suggest these are complex sublayers consisting of spinel and two different chromium oxide phases. We believe this is the clearest structural observation of a spinel phase made to date. During the next part of the passivation process (1–2 h), it is clear that some of the chromium-rich oxide phases are dissolved, exposing metal where selective iron dissolution yields free chromium at the surface. The chromium metal possibly reacts with the passivating agent/additives to form a chromium carbide phase. After 2 h, all of the reactions become kinetically slow and the steels become stable in these conditions.

The effects of citric acid and nitric acid on the 316 coupons are similar to that recorded for Citrisurf. There are, however, some important differences. The maximum in the chromium oxide and spinel phase development appears to be at longer exposure times (3 h) compared to Citrisurf passivation and suggests the Citrisurf is a kinetically faster passivating agent. This can also be seen in the decrease in Fe_2O_3 signal. The citric acid passivation does not appear to reach an “equilibrium” concentration of oxide film products until exposure times of around 4 h. The nitric acid passivation results contrast the citric acid passivators in that the system does not appear to reach an equilibrium composition even after 6 h of treatment. In Fig. 3C, the concentrations of the chromium oxides, spinel, and chromium carbide increase throughout the exposure regime. The iron oxide shows the expected decrease in concentration but then increases through the latter stages of the acid exposure. The final composition (6 h exposure) of the chromium oxides in the passive film is greater than for the citric acid passivators, suggesting thicker passive films are formed. However, the iron oxide results suggest that passivation is not terminated by the process. The data suggest that the nitric acid – produced films are not as effective as citric/Citrisurf – produced films in preventing corrosion.

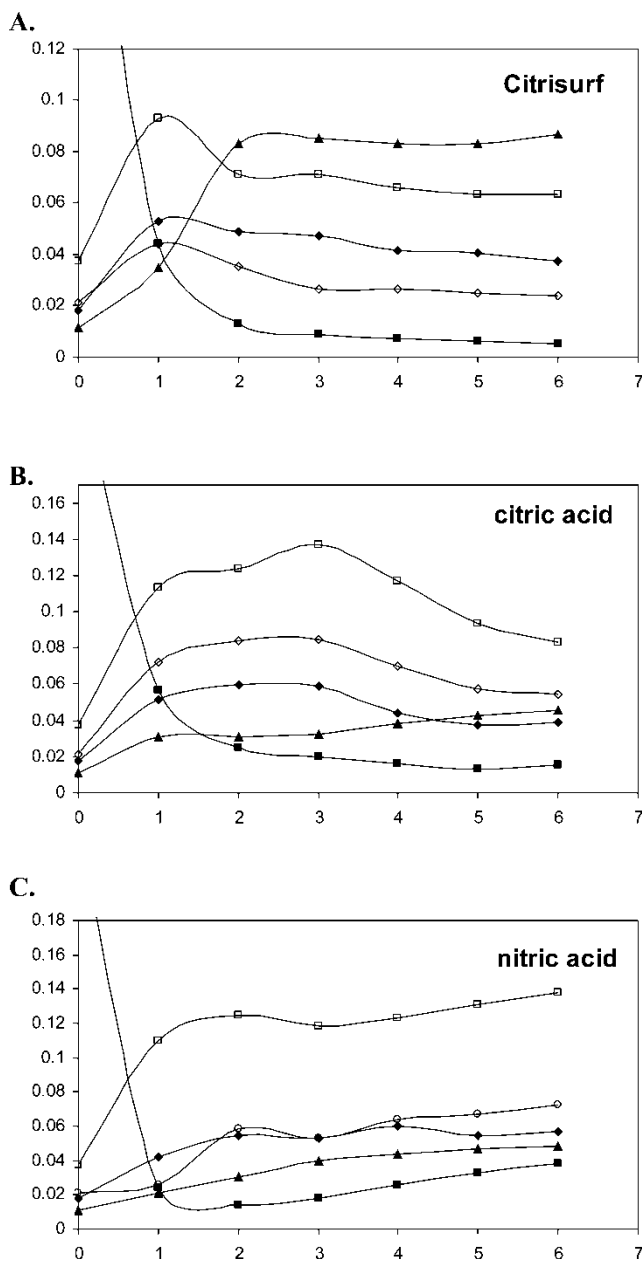


Figure 3. Variation in the reflection intensity (relative to the $\gamma(111)$ reflection) of various phases formed during passivation of 316 steel coupons as a function of exposure time (hours). Data for each passivating agent is shown. \blacklozenge is the spinel phase, \diamond the CrO_2 phase, \blacktriangle the chromium carbide phase, \blacksquare the Fe_2O_3 phase and \square the Cr_2O_3 phase.

3.2.2 304 Coupon Analysis

More obvious for an unpassivated 304 stainless steel (Fig. 2A) is the presence of the spinel phase and α -phase at significantly more concentrations compared to 316 stainless. A previously unobserved Fe_3O_4 ($37.4^\circ 2\theta$, JCPDS file 75-0449) phase can also be seen along with a weak signal from α -ferrite (FeC) at $42.2^\circ 2\theta$ (JCPDS file 03-0411). The Fe_3O_4 at the surface of stainless steels has been seen before, although mixtures of hematite and magnetite are usually seen (Somers and Mittemeijer 1990). The presence of a strong α -phase signal may relate to the initial processing of the coupons, because mechanically developed strain has been shown to promote the formation of this phase (Peterson and Mataya 1997). The 316 is more corrosion resistant than 304 and the data provided here suggest that there are much higher concentrations of nonaustenitic material at the surface of the 304 alloy.

Figure 4 summarizes the PXR analysis of 304 coupons in the three passivating agents (20%) as a function of time. Citrisurf passivation results in the immediate decrease of the spinel, α -, and Fe_3O_4 phases, confirming these are surface materials. The passivation also results in an increase of the Cr_2O_3 phase. This phase and the spinel phase show a broad maximum, suggesting (as above) that these are subsurface layers exposed by passivation. Importantly, the chromium and iron carbide phases increase in concentration on passivation. The formation of iron carbide might result from reaction with the α -phase and therefore is much more easily observed in the 304 experiments. It is clear in the exposure regime that 3 h exposures result in complete passivation of the surface because no further changes in concentrations are observed. Citric acid shows some differences. The first is that the decrease in the α -phase content is not as great as for Citrisurf. This may explain when some of the oxidation products are not seen at as high concentrations as the proprietary passivating agent. Further, it can be seen that many of the passivation products (the oxides, carbides, and spinel) are still increasing after 6 h exposure. This suggests that Citrisurf attains a truly passive layer much more quickly. Nitric acid behaves similarly to citric acid and there is continued increase in the passivation products through the exposures made here. The chromium oxide produced by nitric acid passivation is at a higher concentration than for Citrisurf or citric acid treatments. This suggests that nitric acid results in thicker passive films but also that passivation continues at high exposures. This implies that the passive film is not as effective in preventing further reaction with the acid.

3.3 Surface Analysis

Analysis of the outermost layers of the coupons was made using XPS. Iron 2p $3/2$ photoelectron features were observed at 709.8 eV; this is consistent with iron oxides rather than iron metal. The Cr 2p $3/2$ signal at 575.7 eV is

typical of Cr_2O_3 . The Cr:Fe ratio is derived directly from the $2p\ 3/2$ peak area ratio corrected by the Schofield cross-section (Schofield 1976). In all cases, data were background subtracted using a Shirley-type background (Shirley 1972). A summary of the results is given in Table 1. Similar to the PXR analysis, the surface analysis suggests that the untreated surface has an iron-rich composition. The chromium content in both 304 and 316 steel coupons is significantly greater in the surface region than might be expected from the bulk composition.

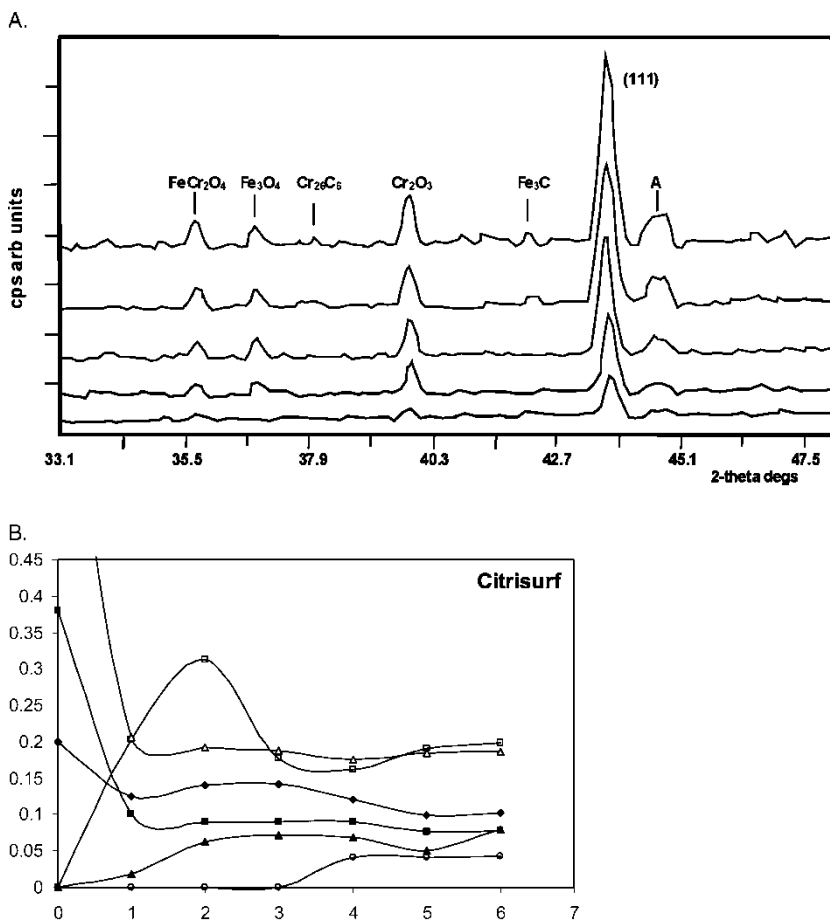


Figure 4. (A) Illustrative PXR data from a Citrisurf passivated 304 coupon as a function of exposure time. Indicates the presence of the Fe α -phase. (B), (C) and (D) Variation in the reflection intensity (relative to the $\gamma(111)$ reflection) of various phases formed during the passivation as a function of exposure time (hours). Data for each passivating agent are shown (20% solutions). \blacklozenge is the spinel phase, \diamond the iron carbide phase, \blacktriangle the chromium carbide phase, \blacksquare the Fe_3O_4 phase, \triangle the α -phase of the steel, and \square the Cr_2O_3 phase.

(Continued)

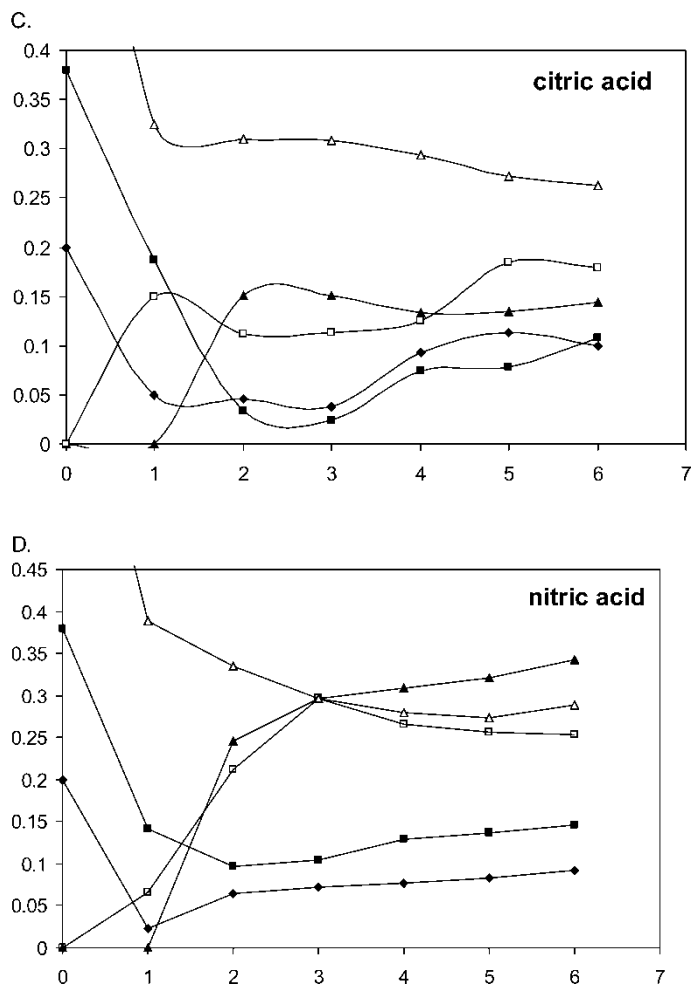


Figure 4. Continued.

Under Al $K\alpha$ radiation, the kinetic energy of outgoing Cr 2p $3/2$ electron is about 911 eV and the inelastic mean free path (i.e., the depth when the signal from the material is $1/e$ of the signal at zero depth) is 2.35 nm, as calculated from Seah and Dench formulism (Shea and Dench 1979). For a passive film formed by mechanical cutting and cleaning, the chromium-rich layer is expected to be somewhere between 1 and 3 nm into the sample (Olsson and Landolt 2003). Consideration of these facts suggests that on the untreated surface, XPS provides information largely relating to the outermost iron-rich layer with some sensitivity to the Cr-rich sublayer.

Passivation in all of the solutions results in an immediate increase in the surface Cr:Fe ratio. After 2 h the passivation results in Cr:Fe ratios of greater

Table 1. Cr/Fe as measured by XPS ratio as a function of passivation treatment for 304 and 316 stainless steel in different conditions

	316 stainless steel			304 stainless steel		
	CS	CA	NA	CS	CA	NA
Untreated	← 0.36 →			← 0.32 →		
2 hours	2.55	2.52	2.3	2.38	2.34	2.16
6 hours	2.63	2.74	3.02	2.42	2.48	2.86

CS, Citrisurf; CA, citric acid; and NA, nitric acid. All passivating agents as 20% solutions.

than 2 on both 316 and 304 coupons. For both 304 and 316 samples after 2 h of passivation, nitric acid results in the lowest Cr:Fe ratios, contradicting the XRF and XRD results. However, following 6 h treatments, the nitric acid exhibits the highest Cr/Fe ratios. It is also clear from the data that passivation using Citrisurf is close to completion after 2 h of treatment. However, this cannot be said of the acid passivators as Cr/Fe ratios rise considerable between 2 and 6 h. We believe that the data show that passivation using the simple acid solutions (in particular, nitric) develop thicker passive films and penetrate deeper into the bulk than for Citrisurf passivation.

3.4 Quantification

The XRF data can be relatively easily quantified, as described above. The intensity of signal is given by a combination of known cross-sections and absorption coefficients. The depth of the analysis is determined by the mass absorption coefficients, which has been detailed above. XRD is somewhat more difficult to quantify. The depth of the analyte within the sample is given by the mass absorption coefficient of Cu K α radiation and the angular terms. Using a Cr20%Fe80% matrix and a linear absorption coefficient of 1750 cm⁻¹, the analyte depths evaluate to about 50, 250, and 500 nm for 1, 5, and 10° incidence angles. However, compared to XRF, calculation of a cross-section is very difficult theoretically. This is because there is a complex structural term that results in several peaks of differing intensity partly determined by geometrical terms. Rather than use a complex matrix of theoretical values, we simply used a relative sensitivity based on physical mixtures. The steels were milled and ground into fine powders and mixed with 10% w/w each of the phases observed. The relative peak intensities are then converted into metal mol % ratio. XPS quantification is outline above. The depth of the analyte is taken as the inelastic mean free path, described above. It should be noted that it is assumed that the entire XPS signal arises from the passive layer and not the bulk metal, thus the chromium enrichment

is calculated directly from the ratios provided in Table 1. This also implies that the iron signal seen arises from the presence of the spinel phase.

The results of the quantification are a depth profile from the combination of nondestructive analysis techniques. Authors have used many techniques to generate depth profiles (Olsson and Landolt 2003). However, these can be limited to the surface region (e.g., angle resolved XPS studies [Lakatos-Varsányi et al. 1998]) or be prone to technique-related mixing of the ions (e.g., secondary ion mass spectroscopy [Calinski and Strehblow 1989]). Thus, it is very difficult to understand the enrichment process. Data are provided in Fig. 5A, which shows the derived depth profiles for 316 stainless steel after

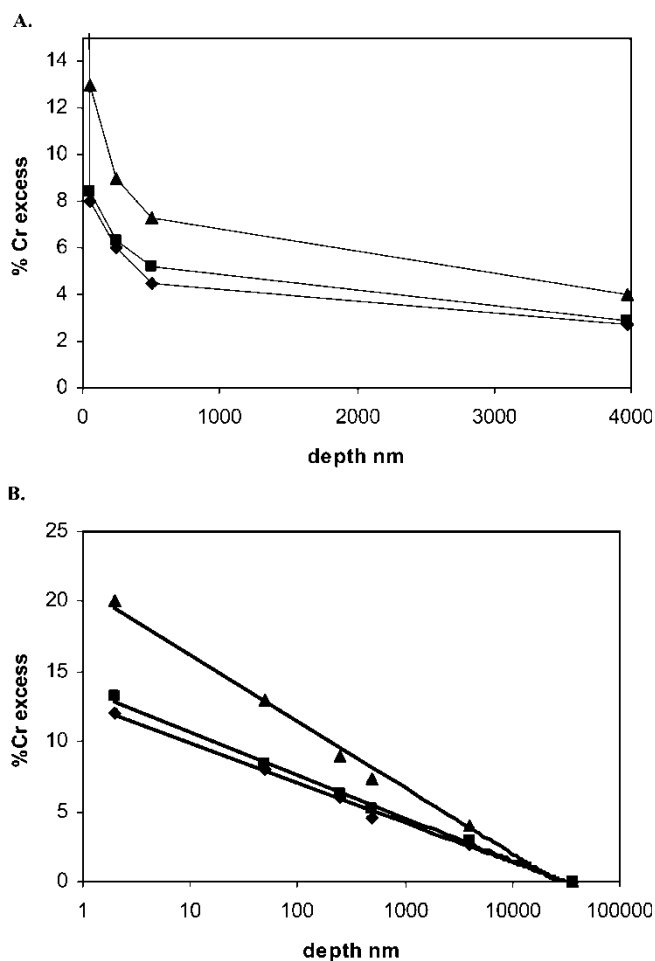


Figure 5. Variation of chromium enrichment (as % above nominal untreated concentration) with depth. See text for details. The data are shown in nonlogarithmic (A) and logarithmic (B) form.

6 h of passivation in a 20% solution of the three passivating agents investigated here. The data are very similar to those obtained for 304 stainless steel, which is not shown for clarity. In the figures, the % chromium is the amount above the composition measured using the XRF L lines, as described above. The L line derived – values are taken as the nominal bulk composition. What are not shown on these plots are the data measured by XPS, which show the surface to be made up of 72.5, 75.5, and 83.2% chromium for the Citrisurf, citric acid, and nitric acid passivations, respectively. The data seem to show an exponential decrease in chromium concentration. However, this form of decay could result in a real trend in the concentration profile or from the exponential nature of the x-ray attenuation process. Figure 5B shows the same data as in logarithmic form. It is clear that the data do not indicate an exponential decay in concentration with depth into the surface, because all points would be related and the y-axis intercept would be close to the value recorded by XPS. The data strongly suggest that, to a large extent, only the surface region is enriched in chromium and that below this enriched layer the alloy has close to the nominal bulk composition. Using the simple model described above, the XRF and XRD data for Citrisurf and citric acid treatment are fully consistent with all of the segregation occurring in the outermost 50 nm of the sample. This is not true for nitric acid passivation because the XRF and XRD suggest significantly higher enrichment values through the whole composition range. This suggests thicker oxide films and some deeper penetration of enrichment into the bulk.

One explanation for the additional penetrative effects of nitric acid compared to the citric acid – based preparations is provided by SEM analysis, shown in Fig. 6. Direct comparison of the effect of 35% solutions of nitric and Citrisurf suggest that nitric acid passivation results in extensive pitting of the surface. For all passivated surfaces, the treatment does lead to grain boundary erosion, and this can be seen in the SEM data shown. However, for nitric acid treatment, large pits and cracks (2–5 μm) can be observed (Fig. 6A), but in higher magnification, smaller pits around 1 μm can be seen in all grains. For Citrisurf passivation, the large pits cannot be observed in any samples, and even under the higher magnification, relatively few pits can be seen and these are all sub-micrometer in size. Pits can extend several micrometer into the surface (Carroll et al. 1989) and would allow preferential iron dissolution through the outer surface passive film. The obvious conclusion to draw is that “over-passivation” is detrimental to the surface and much more likely for nitric acid compared to the citric acid–based passivating agents.

4. CONCLUSIONS

Using several different materials analysis methods, it is shown that highly informative nondestructive depth profiles can be generated by careful quantification procedures. XPS is the simplest method to quantify, since signal intensity is always directly proportional to the amount of material within

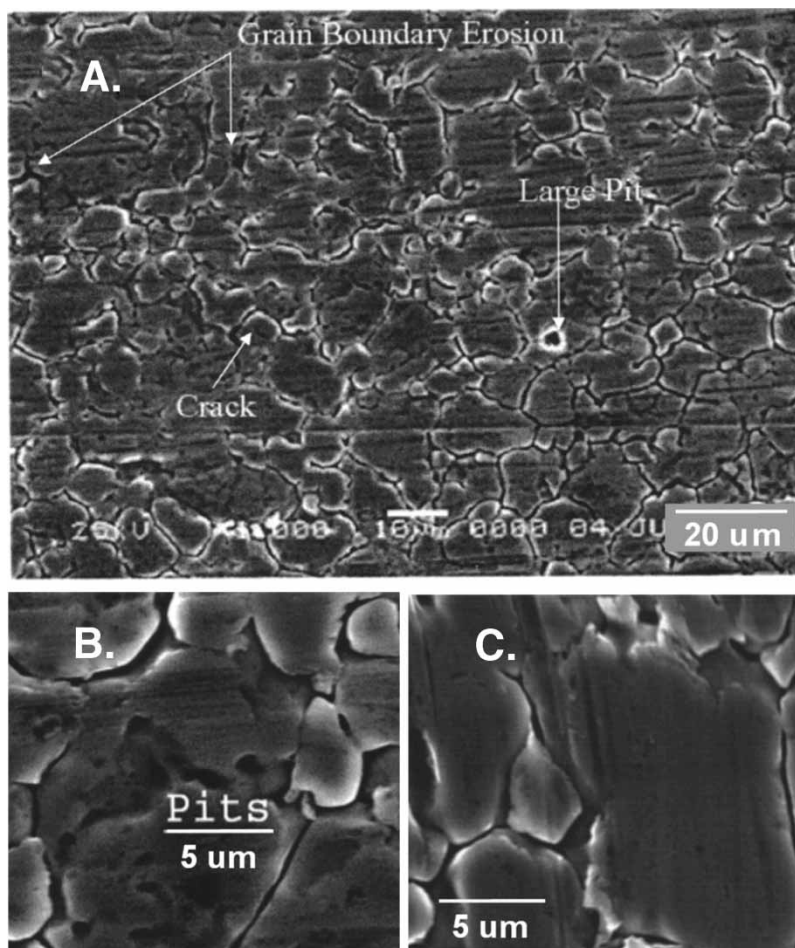


Figure 6. Indicative SEM data from passivated surfaces (35%, 6 h). A and B are from a nitric acid – treated surface and C from a Citrisurf passivated surface.

the analyte and matrix effects play only a minor role in determining the composition. Cross-sections and attenuation lengths are easily obtained. XRF is a more complex analysis method because of strong matrix effects arising from the long penetration of x-rays and absorption within the analyte. However, modelling and established x-ray parameters do allow reasonable “semi-quantitative” estimations to be made. The hardest technique to quantify for simple analysis is PXRD because of the difficulty in estimating diffraction reflection intensities without suitable standards. It should be noted this is possible via techniques such as Rietveld fitting, but this is a highly specialized method and probably not yet appropriate for routine analysis procedures (Bergmann et al. 1997).

REFERENCES

- Askeland, D. 1985. *The Science and Engineering of Materials*, 2nd Ed.; PWS Publishers.
- Bergmann, J., Kleeberg, R., Taut, T., and Haase, A. 1997. Quantitative phase analysis using a new Rietveld algorithm-assisted by improved stability. *Advances in X-ray Analysis*, 40: 112–124.
- Calinski, C. and Strehblow, H.-H. 1989. ISS depth profiles of the passive layer on Fe/Cr alloys. *J. Electrochem. Soc.*, 136: 1328–1331.
- Carroll, W.M., Howley, M.B., and Walsh, T.M. 1989. *Proc. 9th Euro. Congress on Corrosion*, Utrecht, 2–6 October, PFU-226. , European Federation of Corrosion.
- Hicks, D. 1995. *Production and Packaging of Non-Carbonated Fruit Juices and Fruit Beverages*, 2nd Ed.; Van Nostrand Reinhold.
- Kirchheim, R., Heine, B., Hofmann, S., and Hofsäss, H. 1990. Compositional changes of passive films due to different transport rates and preferential dissolution. *Corrosion Science*, 31: 573–598.
- Krause, M.O. 1979. Atomic radiative and radiationless yields for K and L shells. *J. Phys. Chem. Ref. Data*, 8: 307–328.
- Lakatos-Varsányi, M., Falkenberg, M.F., and Olefjord, I. 1998. The influence of phosphate on repassivation of 304 stainless steel in neutral chloride solution. *Electrochim. Acta*, 43: 187–197.
- Lister, D.H., Davidson, R.D., and McAlpine, E. 1987. The mechanism and kinetics of corrosion product release from stainless-steel in lithiated high-temperature water. *Corrosion Science*, 27: 113–140.
- Maller, R.R. 1998. Passivation of stainless steel. *Trends in Food Science and Technology*, 9: 28–32.
- McBee, C.L. and Kruger, J. 1972. Nature of the passive film on Fe-Cr alloys. *Electrochimica Acta*, 17: 1337–1343.
- McMaster, W.H., Kerr, N., Grande, D., Mallett, J.H., and Hubbell, J.H. 1969. Compilation of X-ray cross sections. In *Lawrence Livermore National Laboratory Report*. UCRL-50174, Section II, Revision I.
- Olsson, C.O.A. and Landolt, D. 2003. Passive films on stainless steels—Chemistry, structure and growth. *Electrochimica Acta*, 48: 1093–1104.
- Peterson, S.F. and Mataya, M.C. 1997. Formability of austenitic stainless steel. *JOM – Journal of Minerals, Metals and Materials Soc.*, 49: 54–58.
- Roll, D. 1996. Current methodologies and chemistries utilized in effective passivation procedures, *Proceedings of Interphex 96*, Norwalk, Ct., Reed Exhibition Cos: 134–141.
- Schofield, J.H. 1976. Hartree-Slater subshell photoionization cross-sections at 1254 and 1487 eV. *J. Electron. Spectrosc. Related Phenom.*, 8: 129.
- Shea, M.P. and Dench, W.A. 1979. Quantitative electron spectroscopy of surfaces: a standard data base for electron inelastic mean free paths in solids. *Surf. Interface Analysis*, 1: 2–11.
- Shirley, D.A. 1972. High resolution XPS of the valence band of gold. *Phys. Rev. B.*, 5: 4709–4721.
- Somers, M.A.J. and Mittemeijer, E.J. 1990. Phase transformations and stress relaxation in γ -Fe₄N_{1-x} surface layers during oxidation. *Met. Trans. A*, 21: 901–912.
- Stellwag, B. 1998. The mechanism of oxide film formation on austenitic stainless steels in high temperature water. *Corrosion Science*, 40: 337–370.